SSSAJ

Soil Science Society of America Journal

Vol. 67 No. 5 September–October 2003 SSSJD4 67(5):1319–1630 (2003)

SOIL SCIENCE SOCIETY OF AMERICA JOURNAL

Business and Editorial Offices at
677 South Segoe Road, Madison, WI 53711
(www.soils.org)

Published bimonthly by the Soil Science Society of America, Inc. Periodicals postage paid at Madison, WI, and at additional mailing offices.

Postmaster: Send address change to *SSSA Journal*, 677 S. Segoe Rd., Madison, WI 53711.

Subscription rates (nonmember): $247 per year, within the USA; all others $277. Single copies, $30 USA; elsewhere, $36. Members are eligible for reduced subscription rates. New subscriptions, renewals, and new memberships that include the *SSSA Journal* begin with the first issue of the current year. Claims for copies lost in the mail must be received within 90 days of publication date for domestic subscribers, and within 26 weeks of publication date for foreign subscribers.

Membership in the Society is not a requirement for publication in *SSSA Journal*; however, nonmembers will be charged an additional amount for the first six published pages of a manuscript. To qualify for member rates, at least one author must be an active, emeritus, graduate student, or undergraduate student member of SSSA, CSSA, or ASA on the date the manuscript is accepted for publication.

Volunteered papers will be assessed a charge of $25 per page for nonmembers for each printed page from page one through page six; a charge of $190 per page ($95 per half page) will be assessed all papers for additional pages. No charge will be assessed against invited review papers or comments and letters to the editor. The Society absorbs the cost of reproducing illustrations up to $15 for each paper.

Contributions to the *SSSA Journal* may be (i) papers and notes on original research; and (ii) "Comments and Letters to the Editor" containing (*a*) critical comments on papers published in one of the Society outlets or elsewhere, (*b*) editorial comments by Society officers, or (*c*) personal comments on matters having to do with soil science. Letters to the Editor are limited to one printed page. Contributions need not have been presented at annual meetings. Original research findings are interpreted to mean the outcome of scholarly inquiry, investigation, or experimentation having as an objective the revision of existing concepts, the development of new concepts, or the improvement of techniques in some phase of soil science. Short, critical reviews or essays on timely subjects, upon invitation by the Editorial Board, may be published on a limited basis. Refer to SSSA Publication Policy (Soil Sci. Soc. Am. J. 64(1):1–3, 2000) and to the *Publications Handbook and Style Manual* (ASA-CSSA-SSSA, 1998).

Keep authors anonymous from reviewers by listing title, author(s), author–paper documentation, and acknowledgments on a detachable title page. Repeat manuscript title on the abstract page.

Manuscripts are to be sent to Dr. Richard L. Mulvaney, Editor, *SSSA Journal*, University of Illinois, 1102 South Goodwin Avenue, Urbana, IL 61801 (email: mulvaney@uiuc.edu). Four copies of the manuscript on line-numbered paper are required. All other correspondence should be directed to the Managing Editor, 677 S. Segoe Rd., Madison, WI 53711.

Trade names are sometimes listed in papers in this journal. No endorsement of these products by the publisher is intended, nor is any criticism implied of similar products not mentioned.

ISSN 0361-5995

Suggestions for Contributors to the *Soil Science Society of America Journal*

General Requirements

Contributions to the *Soil Science Society of America Journal* (SSSAJ) may be (i) papers and notes on original research; and (ii) "Comments and Letters to the Editor" containing (a) critical comments on papers published in one of the Society outlets or elsewhere, (b) editorial comments by Society officers, or (c) personal comments on matters having to do with soil science. Notes are not to exceed two printed pages. Letters to the Editor are limited to one printed page. Contributions need not have been presented at annual meetings. Original research findings are interpreted to mean the outcome of scholarly inquiry, investigations, modeling, or experimentation having as an objective the revision of existing concepts, the development of new concepts, or the development of new or improved techniques in some phase of soil science. Authors are encouraged to test modeling results with measurements or published data. Short critical reviews or essays on timely subjects, upon invitation by the Editorial Board, may be published on a limited basis. The SSSAJ also invites submissions for cover illustrations from authors of manuscripts accepted for publication. Refer to SSSA Publication Policy [Soil Sci. Soc. Am. J. 65(1): v–vii. 2001] and to the *Publications Handbook and Style Manual* (ASA–CSSA–SSSA. 1998) for additional information.

The SSSAJ uses a double blind review format. Authors are anonymous to reviewers and reviewers are anonymous to authors. A detachable title page includes title, author(s), author-paper documentation, and acknowledgments. The manuscript title but not the authors are repeated on the abstract page. The *Publications Handbook and Style Manual* (1998) (http://www.asa-cssa-sssa.org/style98/) is the official guide for preparation and editing of papers. Copies are available from ASA Headquarters, 677 S. Segoe Rd., Madison, WI 53711 (books@agronomy.org).

Submitting Manuscripts

Manuscripts can be submitted to the SSSAJ Editor as PDF files. Detailed instructions for creating and uploading PDF files can be found at http://www.manuscripttracker.com/sssaj/ along with instructions related to logging on to the SSSAJ Manuscript Tracker system.

Alternatively, authors may send four legible double-spaced copies of each manuscript on 21.6- by 27.9-cm paper. The lines of type must be numbered on each page, and at least 2.5-cm margins left on top, bottom, and sides. Pages should be numbered consecutively. Type legends for figures (double spaced) on one or more sheets and place at the end of the manuscript.

A cover letter should accompany each submission. Send the copies to:

Dr. Richard L. Mulvaney, Editor
Soil Science Society of America Journal
University of Illinois
1102 South Goodwin Avenue
Urbana, IL 61801
e-mail: mulvaney@uiuc.edu

Potential Reviewers. Authors who submit manuscripts as hard copies or through the SSSAJ Manuscript Tracker system will be encouraged to provide a list of potential reviewers. Those who do not use Manuscript Tracker are encouraged to include a cover letter along with their submission that suggests potential reviewers. Reviewers must not have a conflict of interest involving the authors or paper and the editorial board has the right not to use any reviewers suggested by authors.

Creating the Manuscript Files

Although manuscript review is done electronically or with printed copies, accepted manuscripts are edited as word processing files. Therefore, authors should keep in mind the following when preparing manuscript files.

All accepted manuscript files will ultimately be converted to Microsoft Word format for on-screen editing. Therefore, files that are originally composed in or converted to Microsoft Word are strongly preferred. Other formats are also acceptable, but authors should be aware that errors are occasionally introduced during the conversion process. Furthermore, authors should avoid using word processing features such as automated bulleting and numbering, footnoting, head and subhead formatting, internal linking, or styles. Avoid using more than one font and font size. Limited use of italics, bold, superscripts, and subscripts is acceptable. The file should be double spaced and line numbered, with at least 2.5-cm margins. Rich-text format (.rtf extension) and TEX files are not acceptable.

Title Page. The title page should include:

1. A short title not exceeding 12 words. The title should accurately identify and describe the manuscript content.
2. An author–paper documentation. Include author name(s), sponsoring organization(s), and complete address(es). Identify the corresponding author with an asterisk (*). Professional titles are not listed. Other information such as grant funding, may be included here or placed in an acknowledgment, also on the title page. To ensure an unbiased review, the title page will be removed during the review process. The title, but not the byline, should therefore be repeated on the page that contains the abstract.
3. An abbreviations list. Include abbreviations that are used repeatedly throughout the manuscript. Do not list SI units, chemical element symbols, or variables from equations.
4. The corresponding author's phone and fax numbers and e-mail address.

Abstract. An informative, self-explanatory abstract, not exceeding 250 words (150 words for notes), must be supplied on a separate page. It should specifically tell why and how the study was made, what the results were, and why they were important. Use quantitative terms. The title should be repeated on top of the abstract page without author identification.

Tables. Each table must be on a separate page and numbered consecutively. Do not duplicate matter that is presented in charts or graphs. Use the following symbols for footnotes in the order shown: †, ‡, §, ¶, #, ††, ‡‡, . . . etc.

The symbols *, **, and *** are always used to show statistical significance at 0.05, 0.01, and 0.001 levels, respectively, and are not used for other footnotes. Spell out abbreviations on first mention in tables, even if the abbreviation is defined in the text (i.e., a reader should be able to understand the table contents without referring back to the text).

Figures. Do not use figures that duplicate matter in tables. Photographs for halftone reproduction should be glossy prints with good dark and light contrast. When creating figures, use font sizes and line weights that will reproduce clearly and accurately when figures are sized to the appropriate column width. The minimum line weight is 1/2 point (thinner lines will not reproduce well). Screening and/or shaded patterns often do not reproduce well; whenever possible, use black lines on a white background in place of shaded patterns.

Authors can reduce manuscript length and, therefore, production charges, by supplying photographs and drawings that can be reduced to a one-column width (8.5 cm or 20 picas). Lettering or numbers in the printed figure should not be smaller than the type size in the body of an article as printed in the journal (8-point type) or larger than the size of the main subheads (12-point type). The minimum type size is 6-point type. As an example, a 17-cm-wide figure should have 16-point type, so that when the figure is reduced to a single column, the type is reduced to 8-point type.

Label each figure with the title of the article and the figure number. Type captions in the word processing file following the references. As with tables, spell out abbreviations on first mention in figure captions, even if they have already been defined in the text.

References. When preparing the reference list, keep in mind the following:

1. Do not number the references listed.
2. Arrange the list alphabetically by the names of the first authors and then by the second and third authors.
3. Single-authored articles should precede multiple-authored articles for which the individual is senior author.
4. Two or more articles by the same author(s) are listed chronologically; two or more in the same year are indicated by the letters a, b, c, etc.
5. All published works referred to in the text must be listed in the reference list and vice versa.
6. Only literature that is available through libraries can be cited. The reference list can include theses, dissertations, and abstracts.
7. Material not available through libraries, such as personal com-

munications or privileged data, should be cited in the text in parenthetical form.
8. Chapter references from books must include, in order, authors, year, chapter or article title, page range, editor(s), book title, publisher, and city.
9. Symposium proceedings should include editor, date and place of symposium, publisher, and page numbers.

Style Guidelines

All soils discussed in publications should be identified according to the U.S. soil taxonomic system the first time each soil is mentioned. The Latin binomial or trinomial and authority must be shown for all plants, insects, pathogens, and animals when first mentioned. Both the accepted common name and the chemical name of pesticides must be provided. SI units must be used in all manuscripts. Corresponding metric or English units may be added in parentheses at the discretion of the author. If a commercially available product is mentioned, the name and location of the manufacturer should be included in parentheses after first mention.

Official Sources

1. Spelling: Webster's *New Collegiate Dictionary*
2. Amendments to the U.S. system of soil taxonomy (Soil Survey Staff, 1975) have been issued in the *National Soil Survey Handbook* (NRCS, 1982–1996) and in *Keys to Soil Taxonomy* (Soil Survey Staff, 1996). Updated versions of these and other resources are available at http://www.statlab.iastate.edu/soils/index.html
3. Scientific names of plants: *A Checklist of Names for 3000 Vascular Plants of Economic Importance* (USDA Agric. Handb. 505, see also the USDA Germplasm Resources Information Network database, http://www.ars-grin.gov/npgs/searchgrin.html)
4. Chemical names of pesticides: *Farm Chemicals Handbook* (Meister Publishing, revised yearly)
5. Soil series names: *Soil Series of the United States, Including Puerto Rico and the U.S. Virgin Islands* (USDA-SCS Misc. Publ. 1483, http://www.statlab.iastate.edu:80/soils/osd)
6. Fungal nomenclature: *Fungi on Plants and Plant Products in the United States* (APS Press)
7. Journal abbreviations: *Chemical Abstracts Service Source Index* (American Chemical Society, revised yearly)
8. *The Glossary of Soil Science Terms* is available both in hard copy (SSSA, 1997) and on the SSSA Web page (www.soils.org/sssagloss/). It contains definitions of more than 1800 terms, a procedural guide for tillage terminology, an outline of the U.S. soil classification system, and the designations for soil horizons and layers.

Manuscript Revisions

Authors have three months to make revisions and return their manuscripts following reviewer and associate editor comments. If not returned within three months, the manuscript will be released; it must then be resubmitted as a new paper.

Length of Manuscript and Page Charges

Membership in the Society is not a requirement for publication in the SSSAJ; however, nonmembers will be charged an additional amount for the first six published pages of a manuscript. To qualify for member rates, at least one author must be an active, emeritus, graduate student, or undergraduate student member of SSSA, CSSA, or ASA on the date the manuscript is accepted for publication. Volunteered papers will be assessed a charge of $25 per page for nonmembers for each printed page from page one through page six; a charge of $190 per page ($95 per half page) will be assessed all papers for additional pages. No charges will be assessed against invited review papers or comments and letters to the editor. The Society absorbs the cost of reproducing illustrations up to $15 for each paper.

In general, four manuscript pages will equal one printed page. For space economy, Materials and Methods, long Literature Reviews, theory, soil or site descriptions, etc., footnotes, tables, figure captions, and references are set in small type. Each table and figure will usually take 1/4 of a printed page. For tabular matter, 9 lines of typewritten matter equal 1 column-inch of type. Allow also for rules and spacing. Tables with more than 35 units (including space between words) in a horizontal line can rarely be set 1 page-column wide. The depth of a printed figure will be in the same proportion to the width (1 column = 8.5 cm; 2 column = 17.2 cm) as that of the corresponding dimensions in the original drawing.

Authors can publish color photos, figures, or maps at their own expense. Please call the Managing Editor (608-273-8095) for price information.

Accepted Manuscripts

Following hard copy submission and review, both a printed copy and word processing file of the final accepted manuscript are required. The printed copy and word processing file must match exactly in all parts of the manuscript. Printed copies and files for tables and figures must also be included. The files for text, tables, and figures should be separate.

Send the printed copy and a disk with the manuscript files to:

Nicholas Rhodehamel, Managing Editor, SSSAJ
American Society of Agronomy
677 South Segoe Road
Madison, WI, USA 53711

Alternatively, if the paper was submitted for review through the SSSAJ Manuscript Tracker system, the final accepted version can be uploaded as a Word file at http://www.manuscripttracker.com/sssaj/finaldocs.htm. A printed copy that exactly matches the word processing file must still be sent to the address listed above.

Questions? Send your questions to Nicholas Rhodehamel, Managing Editor, SSSAJ (nrhodehamel@agronomy.org).

July 2002

SSSAJ September–October 2003 Vol. 67, No. 5

Soil Science Society of America Journal

Continued on page ii

This issue's cover: Kurt Johnsen of the USDA Forest Service, Southern Research Station employs an air-knife to remove soil from a *Pinus taeda* root system. Destructive sampling is time-consuming, but necessary to assess belowground allocation and distribution of carbon in woody roots. Ground-penetrating radar can be used to augment traditional belowground biomass harvests noninvasively. See "Utility of Ground-Penetrating Radar as a Root Biomass Survey Tool in Forest Systems" by J. Butnor, J.A. Doolittle, K.H. Johnsen, L. Samuelson, T. Stokes, and L. Kress, p. 1607–1615. The article is part of a symposium entitled, "Approaches and Technologies for Detecting Changes in Forest Soil Carbon Pools." Photo credit: John Butnor, USDA Forest Service, Southern Research Station.

Continued from page i

Important Note to Authors

Recently, the *SSSAJ* production editing staff has changed systems for preparing accepted manuscripts for typesetting.

The new, more efficient system requires Microsoft Word documents rather than Corel WordPerfect. We strongly encourage you to compose manuscript files in Word.

In addition, the new system can use Word tables. Fewer errors are induced when tables are set from electronic files than, as was formerly done, from hard copy.

Figures are still prepared almost entirely from hard copy. You may compose figures in any software you desire; submit these files but also send hard copies.

For more information, see the updated *Suggestions to Contributors*, this issue of *SSSAJ* and http://soil.scijournals.org/misc/ifora.shtml.

SOIL SCIENCE SOCIETY OF AMERICA
JOURNAL

VOL. 67 SEPTEMBER–OCTOBER 2003 No. 5

DIVISION S-1—SOIL PHYSICS

Electrical Resistivity Imaging for Detecting Soil Cracking at the Centimetric Scale

Anatja Samouëlian,* Isabelle Cousin, Guy Richard, Alain Tabbagh, and Ary Bruand

ABSTRACT

Electrical resistivity measurements at high resolution (1.5-cm electrode spacing) were performed to detect, from the soil surface, small cracks developing within the soil. We recorded a vertical electrical pseudo-section in a decimetric undisturbed homogenous soil block (silt loam) for different artificial cracking stages. Because of the unusually reduced electrode spacing associated with an air-dried soil surface, a specific Cu/$CuSO_4$ electrode was designed for precision wet contact at given points. The apparent resistivity measurements of the pseudo-section and the interpreted data inverted by using the Res2Dinv software are discussed. The range of interpreted electrical resistivity associated with cracking is considerable, (from 168 to 2185 Ω m) because the cracks are filled with air that is an infinitely resistant medium. Results showed that even small structures cause perceptible changes in resistivity that can be detected by the electrical resistivity method. Results also showed that specific software is required to predict real crack depth.

On arable land, soil can be compacted by traffic, hard setting, and crusting processes. Soil structure can be regenerated after compaction by tillage operations, biological processes, and climate processes. With new agricultural practices such as reduced tillage or no-tillage, soil structure mostly regenerates via natural processes. Thus, better understanding of climate effects is needed, especially the ability for soil to recover porosity by crack formation due to swelling and shrinking. Voorhees (1983) pointed out the role played by natural processes, such as soil freezing and thawing, and wetting and drying, decrease penetration resistance in the tilled layer of a compacted soil by about 50%, depending on soil water content. Mackie-Dawson et al. (1989) studied the evolution of the cracking system in the first 10 cm of soil by using vertical image analysis. They observed significant soil structural changes during an annual cycle of drying and wetting. Up to now, crack networks have been described traditionally, either by measuring manually in the field the crack geometry that forms at the soil surface (Blackwell et al., 1985; Lima and Grismer, 1992; Ringrose-Voase and Sanidad, 1996; Tuong et al., 1996), or automatically by using two-dimensional image analysis (Bullock and Murphy, 1980; Hallaire, 1984; McGarry et al., 2000; Scott et al., 1986; Stadler et al., 2000; Stengel, 1988; Velde et al., 1996). Image analysis was widely used to calculate morphological parameters of cracks. VandenBygaart et al. (1999) performed microscopic observations and showed a development of soil structure with time in an 11-yr chronosequence of no-tillage. They noticed that the number of horizontally oriented elongated macropores in the top 5 to 15 cm increased because of the absence of tillage and of the combination of annual freeze–thaw processes. McGarry et al. (2000) assessed soil structure from traditional and zero-till treatments in a Vertisol. They recorded a greater volume of large pores (1.5- to 3-mm equivalent diameter in size) after 8 yr of zero-till and a greater volume of pores of smaller size (0.74- to 1.0-mm equivalent diameter) after 8 yr of traditional tillage.

Models that are based on these experimental observations and that describe crack growth are already available. Horgan and Young (2000) developed a two-dimensional empirical model based on random processes whose parameters are not directly related to the properties of a real soil. Perrier et al. (1999) used fractals to describe the cracking patterns that appeared in a homogeneous soil. Chertkov and Ravina (1998) developed a physically based probabilistic model of crack network geometry and observed a good agreement with one-dimensional experimental data. Hallaire (1988) used image analysis to describe a three-dimensional model with cubic geometry and isotropic shrinking.

However, because the tensile and shearing stresses

A. Samouëlian and I. Cousin, INRA, Unité de Science du Sol, Avenue de la Pomme de Pin, BP 20619, 45166 Olivet, Cedex, France; G. Richard, INRA, Unité d'Agronomie, Rue Fernand Christ, 02007 Laon Cedex, France; A. Tabbagh, UMR 7619 "Sisyphe", Case 105, 4 place Jussieu, 75005 Paris, France; A. Bruand, ISTO, Université d'Orléans, Géosciences, BP 6759, 45067 Orléans Cedex 2, France. Received 1 July 2002. *Corresponding author (samouelian@orleans.inra.fr).

Published in Soil Sci. Soc. Am. J. 67:1319–1326 (2003).

677 S. Segoe Rd., Madison, WI 53711 USA

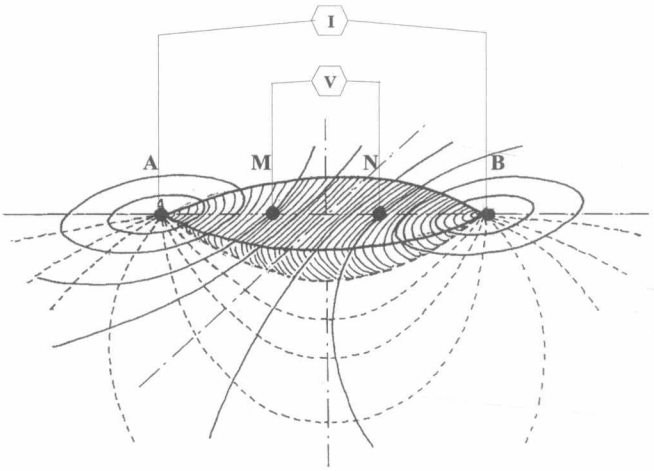

Fig. 1. Electrical distribution of current lines (dashed) and equipotential surface between two current electrodes A and B; measure of electrical potential across the electrodes *M* and N in a Wenner configuration.

vary in a soil with depth, we cannot realistically deduce soil behavior from the description of the surface alone. As a consequence, geometry of a crack network cannot be deduced from a two-dimensional description and geometrical analyses must provide three-dimensional information. In addition, most studies have used two-dimensional vertical data obtained with destructive techniques, thus restricting the potential of these techniques for monitoring crack development. Therefore, the understanding of the dynamic processes of crack pattern growth requires the collection of three-dimensional data on a soil volume by using a non-destructive imaging technique. Electrical resistivity imaging is a geophysical investigation tool that has been used for many decades in hydrogeology, mining, oil and civil engineering, and archaeological prospecting. The technique is particularly useful in the study of complex geology (Griffiths and Barker, 1993), and has also been used for shallow subsurface investigation and environmental works (Hesse et al., 1986) as well as archaeological (Delapierre, 1998) and pedological surveys (Bourennane et al., 1998; Lamotte et al., 1994; Tabbagh et al., 2000). Electrical resistivity varies considerably according to the electrical conductivity of materials and their proportions in a soil volume. Dannowski and Yaramanci (1999), Goyal et al., (1996), Hagrey and Michaelsen (1999), Michot et al., (2000), and Zhou et al., (2001) related electrical resistivity to soil water content in their experiments. Acworth (1999) used this method to identify zones of high salt content in a clay layer. In these studies the electrical anomalies corresponded to large objects (i.e., larger than a decimetric size). Our objective is to adapt this method to identify small heterogeneities (i.e., objects of millimetric size) related to soil structure and especially to cracks developing during drying and wetting cycles. Since a crack in a drying context is air-filled, this structure should be easily detectable because of the infinite electrical resistivity of air. Consequently, we examined the ability of electrical resistivity surveys to distinguish small resistivity anomalies, with specially designed electrodes. This paper describes the first experiment to test the feasibility of electrical resistivity monitoring at this scale.

Principle of Electrical Measurement Profile

The general principle behind geophysical exploration is to collect data external to the medium under investigation but that are functions of the internal properties of this medium (Scollar et al., 1990). Andrews et al. (1995) defined electrical imaging as a picture of the electrical properties of the subsurface by passing an electrical current along many different paths and measuring the associated voltage. In the resistivity method, artificially generated electric currents are injected into the ground and the resulting differences of potential are measured at the surface. In practice, current I (A) is injected into the ground through two electrodes A and B, and an electrical potential ΔV (V) is measured across a second pair of electrodes M and N (Fig. 1). In a homogenous terrain, the current is distributed in the ground between Points A and B with a regular geometric shape. In this distribution, the lines of current linking A and B and the equipotential surfaces which are close to hemispherical shape near A and B, cross each other. Current density is not equal at all points, and the main part of intensity I emitted between A and B is concentrated in the hachured volume in the neighborhood of the AB segment (Fig. 1). This zone is related to the "higher sensitivity region" of the quadripole. This volume becomes larger as the distance AB increases. Soil apparent resistivity (ρ) is calculated for a quadripole electrode (Fig. 1) as following:

$$\rho = \frac{\Delta V}{I}\left(\frac{2\pi}{(1/\mathrm{MA} - 1/\mathrm{MB} + 1/\mathrm{NB} - 1/\mathrm{NA})}\right) = K\frac{\Delta V}{I} \quad [1]$$

where ρ is in (Ω m), MA, MB, NB, NA are the interelectrode spacing (m), I the injected current, and ΔV the measured electrical potential (Scollar et al., 1990). This equation enables the determination of soil resistivity from four electrodes placed randomly on the surface. Constant K is the geometric coefficient of the quadripole. In the case of the Wenner array, the electrodes are arranged in line and the current and potential electrodes are kept at an equal spacing a (m). Then, the geometric factor K becomes $K = 2\pi a$. The depth of investigation is a function of the distance between the nearest potential and current electrodes. The separation between the electrodes mainly determines the volume of soil detected by the instrument. The greater is the electrode spacing, the deeper is the investigation. The resistivity value is conventionally attributed to the geometric center point of the experimental array.

When the soil is not electrically homogeneous, the current lines and equipotential surfaces are distorted. Their patterns are no longer as described in Fig. 1. In this case, the resistivity measurement, obtained from ΔV and I, is called the apparent resistivity ρ_a. The latter is calculated with Eq. [1], and it provides qualitative

information on the soil considered as a homogeneous equivalent medium.

MATERIALS AND METHODS

The Soil Studied

The experiments were conducted in the laboratory on an air-dried soil sample (2.4 by 1.7 by 1.6 dm^3) with an initial massive structure resulting from severe compaction by wheel traffic. The sample was collected in the tilled horizon of a silt loam (Typic Hapludalf) located on an experimental site in the National Institute for Agronomic Research Center at Mons en Chaussée (Somme, France) (Richard et al., 2001). An apparent vertical two-dimensional electrical resistivity pseudo-section was first measured along a 21-cm line from the top surface of the soil block (Stage A with no crack). Then cracks were made manually. In terms of electrical prospecting, the crack is air-filled and corresponds to a resistant structure. A crack of 2-mm width and varying depths (1, 2, 3, and 4 cm deep) was created artificially with a saw to obtain four cracking stages (B, C, D, and E) in the soil sample. The physical model used for soil fractures was intentionally simplistic because this experimentation consists in a feasibility test of electrical measurements. All the measurements were conducted on the soil sample the same day under controlled conditions (room temperature 22°C). The experiment lasted 4 h and the volumetric water content was 0.09 cm^3cm^{-3} and remained stable throughout the experiment. The variation of resistivity was then related to the variation of the structure alone.

Microelectrodes

Our experiment focused on the top 10 cm of the soil, thus the electrical array required centimetric interelectrode spacing. Because of the unusually close electrode spacing associated with an air-dried soil surface, a specific electrode device was designed to improve the electrical contact between the dried soil surface. Indeed, classical electrodes such as metal needles do not permit a correct electrical contact with a soil when it dries. We then designed a new electrode that enables a wet contact between the electrode and the soil surface. Figure 2 shows this specific electrode, manufactured from a small-saturated cone-shaped ceramic cup (2-mm external diameter) linked to a Cu/$CuSO_4$ complex. The copper wire had a section of 0.6 mm, and the concentration of the $CuSO_4$ solution was 0.05 mol L^{-1}. The ceramic cup was joined to a transparent plastic rigid tube (3-mm external diameter and 2-mm internal diameter). The saturated ceramic cup placed on the soil surface permitted a wet contact. Blotting paper protected the soil surface during the installation of the device, so that all the electrodes reached the soil surface at the same time when the paper was removed. The measurements were performed as soon as the electrodes were placed in contact with the soil, to avoid variation of the electrical response of the soil because of infiltration of some $CuSO_4$ solution in the soil porosity.

Two-Dimensional Vertical Pseudo-Section

To detect the crack, its lateral position and its depth, a 21-cm line of 15 electrodes each separated by a constant distance *a* (1.5 cm) was installed at the soil block surface. The crack was located between Electrodes 8 and 9. A Wenner array was used to monitor the electrical potential (Fig. 3). The first four electrodes 1, 2, 3, and 4 were connected as A, M, N, and B (Station 1). A second measurement was performed by disconnecting the first four electrodes and moving the array along the 21-cm measurement line by a single electrode spacing *a*

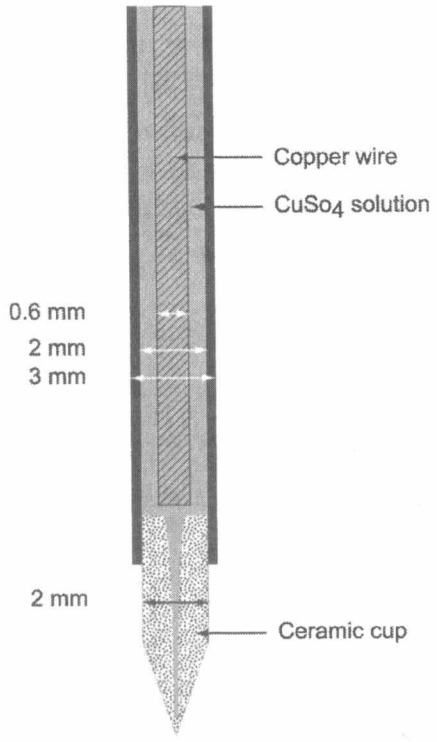

Fig. 2. Electrode device.

and connecting the array to Electrodes 2, 3, 4, and 5. The process was repeated until reaching the end of the line. Then a second profile was recorded by connecting the electrodes in a way that A, M, N, and B occupied electrode positions 1, 3, 5, and 7 (Station 2). The array was then moved along the line by a 2*a* spacing. The process was repeated by increasing the electrode spacing each time by multiple N of the initial electrode spacing, which resulted in four depth measurements. For each measurement, the selection of electrodes connected to the resistivity meter (Syscal-R1 Plus, Iris Instrument, Orléans, France) was controlled by an automatic computer-controlled switch array (Multinode). Intensity *I* injected through the A and B electrodes varied from 2 to 3.5 mA while the electrical potential varied from 251 to 3231 mV. With this configuration, 12, 9, 6, and 3 measurements were performed as the spacing multiple N increased from 1 to 4. The measured values were plotted on a measurement map at the intersections of lines sloping at 45° from the centers of the quadripole. The values were thus plotted along the depth, which reflects the

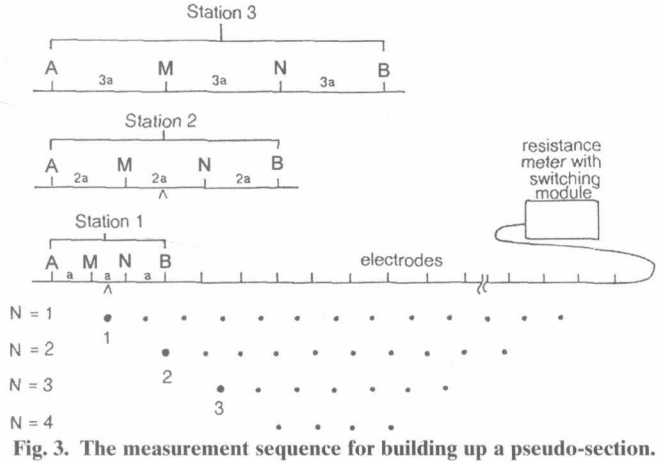

Fig. 3. The measurement sequence for building up a pseudo-section.

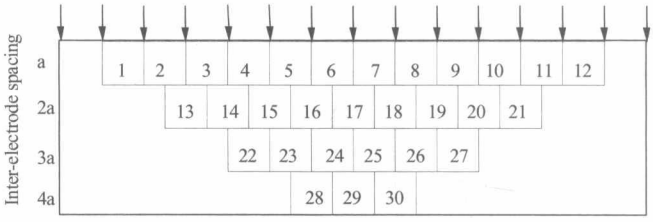

Fig. 4. Measurement map of an apparent electrical resistivity pseudo-section in a Wenner configuration of 15 electrodes.

increasing depth of current penetration as the interelectrode spacing a increased. It should be noted that the units on the vertical axis of the measurement map (Fig. 4) are multiple values of the interelectrode spacing a, from a to $4a$. Thus, there were 30 separate apparent resistivity measurements. As the interelectrode spacing a increased, the measurements sampled increasingly greater depths and increasingly greater volumes of soil. In other words, the total soil volume affected by the current injection rose as the interelectrode spacing a increased. The measurement was plotted beneath the center of the four electrodes.

Resistivity Inversion

The heterogeneities that are present in a soil disturb the theoretical current distribution. The electrical measurement involves a given volume of soil within which the presence of heterogeneity affects the overall measured value. Thus the pseudo-section of apparent resistivity gives a qualitative spatial distribution of electrical resistivity in vertical cross-section. A quantitative approach therefore requires a mathematical inversion of the apparent electrical resistivity into interpreted resistivity. Numerical inversion of the experimental apparent resistivity was performed using Res2Dinv software (Loke and Barker, 1996). This software is widely used in electrical surveys (Acworth, 1999; Delapierre, 1998; Michot et al., 2000). This method is based on the smoothness-constrained least squares method applied to apparent electrical resistivity. The volume of influence described by the apparent resistivity is translated into the depth of investigation related to the interpreted resistivity. The two-dimensional model divides the subsurface into a number of rectangular blocks as shown in Fig. 5. Regarding the Wenner array, the thickness of the first layer of blocks is based on experimental results (Edwards, 1977). The depth corresponds to the "median depth of investigation" $a/2$. The thickness of each subsequent deeper layer is increased normally by 10%. Figure 6 shows the successive stages of the inversion method. Initially, an interpreted resistivity pseudo-section is calculated from the measured apparent resistivity

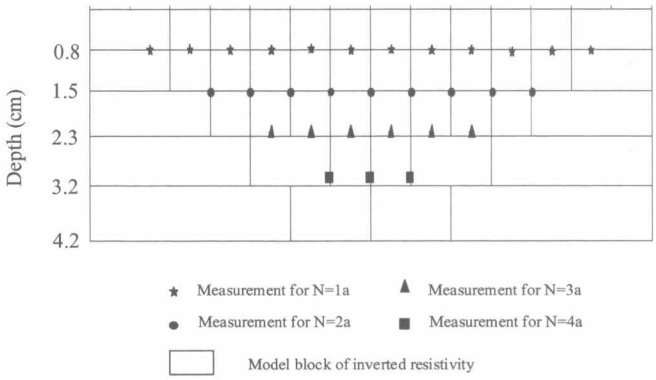

Fig. 5. Arrangement of model blocks and apparent resistivity data points in a Wenner array.

pseudo-section. The second stage then consists in resolving the direct problem (i.e., in calculating the apparent resistivity pseudo-section from the inverted resistivity pseudo-section previously obtained in the first stage). In the third stage, the algorithm calculates the difference between the measured and calculated apparent pseudo-sections. An iterative process is performed until the difference became small enough. The optimization method reduces the differences between the calculated and measured resistivity values by adjusting the resistivity of the model blocks. The measurement of this difference is given by the root mean square error (RMSE) as following:

$$\mathrm{RMSE} = \sqrt{\frac{1}{n}\sum_{i=1}^{n}(\rho_c - \rho_m)^2} \qquad [2]$$

where ρ_c, ρ_m, and n are respectively the apparent resistivity simulated by the Res2Dinv software, the apparent resistivity measured during the experiment and the number of data points.

RESULTS

Apparent Resistivity Interpretation

Figure 7 shows the apparent electrical resistivity pseudo-sections for the cracking Stages A, B, C, D, and E. The set of five profiles describes the artificial growth of the crack located between Electrodes 8 and 9. Map representations are only based on experimental values. No interpolated values were added. Consequently, each mesh represented a data point value corresponding to a Wenner array. Stage A represented the initial soil massive structure, without any crack. The corresponding electrical pseudo-section exhibited a homogeneous apparent resistivity of 47 Ω m. The further Stages B, C, D, and E, presented electrical differentiations directly above the crack between Electrodes 8 and 9. The deeper was the crack in this configuration, the higher was the apparent resistivity. The resistivity range varied from 52 to 77 Ω m. Another demonstration of the resistivity modification can be represented by positive electrical anomaly (Fig. 8). The resistivity anomaly was calculated as following:

$$\Delta\rho_a = \frac{(\rho_{a,X} - \rho_{a,A})}{\rho_{a,A}} \qquad [3]$$

where $\rho_{a,A}$ and $\rho_{a,X}$ were respectively the apparent resistivity of the initial Stage A and the apparent resistivity of the different cracking growing stages (X = B, C, D, or E). All four individual pseudo-sections showed a similar anomaly distribution. Directly above the crack, the positive anomaly varied from 38 to 104% respectively for Stages B and E. Our results also showed that not only the amplitude of the apparent resistivity anomalies increased as the crack grew, so did also its downward extension. The classical reversed V-shape on the map corresponded to a vertical plane electrical discontinuity. Both the apparent resistivity and the anomalies (Fig. 7 and 8) remained constant outside the area of crack influence. This is consistent with no variation of the water content in the soil block throughout experimentation and confirms that the electrical resistivity measurement was affected by variation of the soil struc-

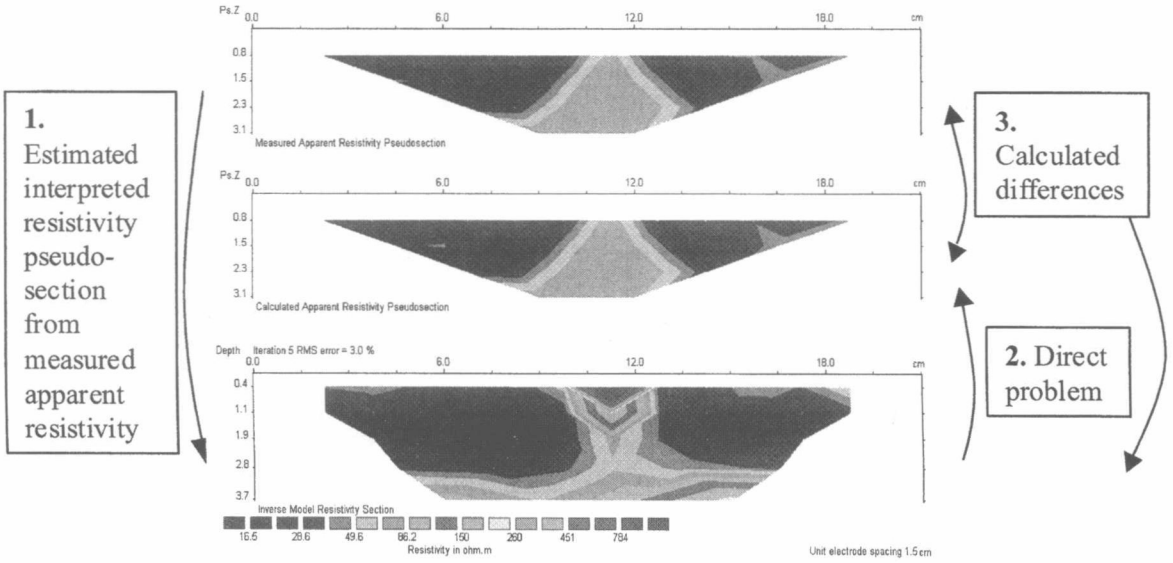

Fig. 6. Mathematical inversion of Res2dinv model.

ture alone in our experiment. As expected, the positive anomaly corresponded to the electrical crack signature, as a resistant object that could be detected by resistivity measurement.

Quantitative Resistivity Interpretation: Resistivity Inversion

The measured apparent resistivity pseudo-sections were analyzed by using the Res2Dinv software to calculate interpreted resistivity pseudo-sections. The latter are shown in Fig. 9 for Stages A, B, C, D, and E. In our case, five iterations for the inversion were usually enough to derive a model distribution producing a result with an RMSE lower than 5%. Initial soil block resistivity at Stage A was relatively homogenous being equal to 37 Ω m. For Stages B, C, D, and E, the calculated interpreted resistivity clearly showed zones of higher electrical resistivity, from 168 to 2185 Ω m between the Electrodes 8 and 9. This high resistivity was directly correlated with the growing crack 1 to 4 cm deep. The highest heterogeneity amplitude was located at 0.8-cm depth. The magnitude of the interpreted variation decreased as the electrode spacing increased.

Figure 10 illustrates the vertical sensitivity of interpreted resistivity during cracking stages. The variation of crack depth from 1 to 4 cm influenced electrical resistivity distribution. The interpreted resistivity, in the first 0.8-cm depth, increased from 168 to 2185 Ω m as the crack grew from 1 to 4 cm. The electrical resistivity in the second horizontal layer (0.8- to 1.5-cm depth) rose by 10% between Stages B (32 Ω m) and E. Beyond the 1.5-cm depth layer, resistivity remained stable even for a 4-cm crack depth. The first horizontal layer was the most sensitive to structural changes.

Figure 11 illustrates the horizontal sensitivity of interpreted resistivity during cracking stages for the first depth layer (0–0.8 cm). Stage A, represented the initial soil structure without any crack or any significant electrical variation. Directly above Electrodes 8 and 9, the electrical signature of the crack increased as the crack grew, as shown in Fig. 10. The lateral sensibility is related to the following point measurement, 1.5-cm apart. Progression was the same for all cracking stages, B, C, D, and E, characterized by decreased electrical resistivity in the crack site. The decrease was highest for Stage E, corresponding to a fall of 98% at the 1.5-cm distance. The resistivity contrast between the crack and the soil was abrupt. The lateral influence of the 2-mm width vertical crack was negligible.

DISCUSSION

This experimental survey focuses on electrical resistivity response from subsurface varying structures. Analyzing the vertical interpreted pseudo-sections revealed the presence of high resistivity contrasts in a vertical zone located at the position of the crack, between Electrodes 8 and 9. This demonstrated the effect of soil structure on the electrical resistivity measurement. The new ceramic cup electrodes enabled efficient electrical monitoring in dry soil. Although the shortest interelectrode spacing was 1.5 cm the principle of point source electrical measurement was respected owing to the wet contact at the soil surface through the small (millimeter) electrodes.

Experiment conditions warranted stable water content during measurements. Göbel et al. (1993), Hagrey and Michaelsen (1999), and Michot et al. (2000) studied the variation of electrical resistivity in the subsurface in water infiltration experiments. The range of interpreted resistivity measurement varied from low resistivity 10 Ω m, corresponding to wet conditions, to 200 Ω m for dry conditions. In our experiment, high and abrupt electrical resistivity measurements ranging from 48 to 2185 Ω m were recorded and attributed to the artificial crack. The crack was filled with air and represented a resistant structure in terms of electrical prospecting. The interpreted resistivity pseudo-sections permitted detection of crack location between Electrodes 8 and 9, on the one hand, and crack vertical orientation on the other

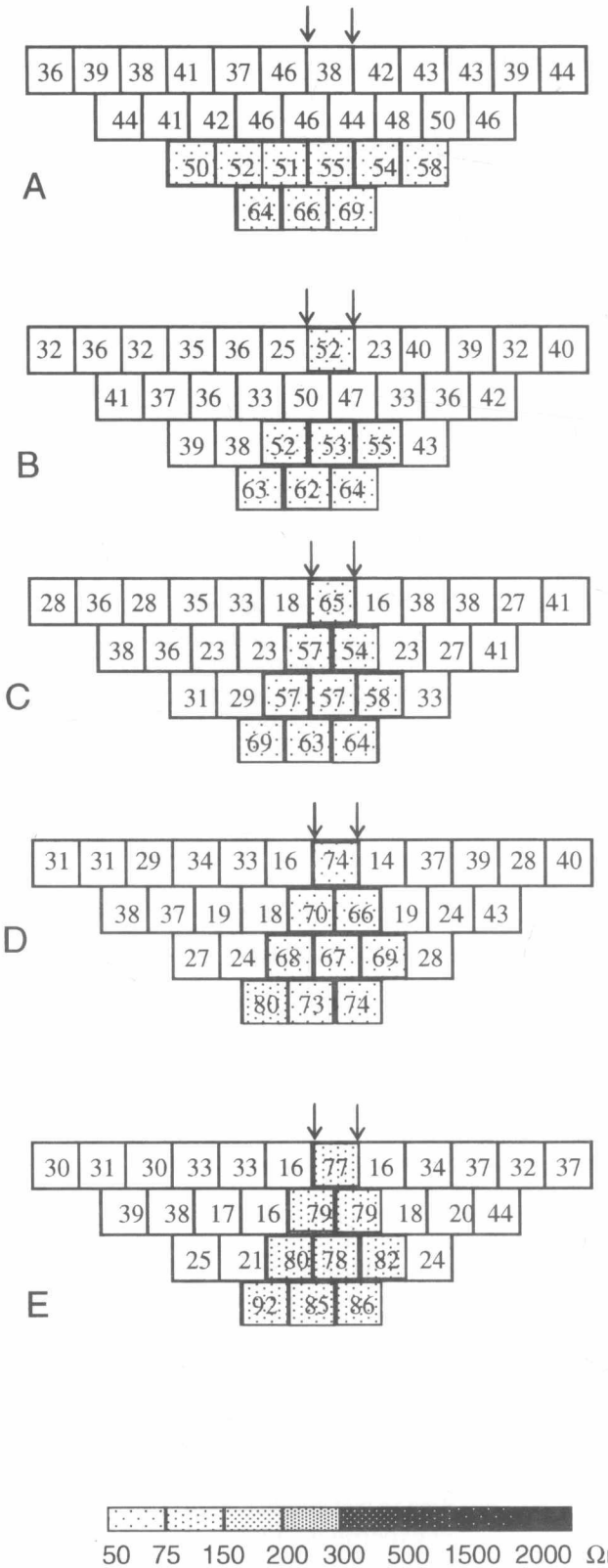

Fig. 7. Apparent resistivity pseudo-section for the five stages, crack localization between the Electrodes 8 and 9.

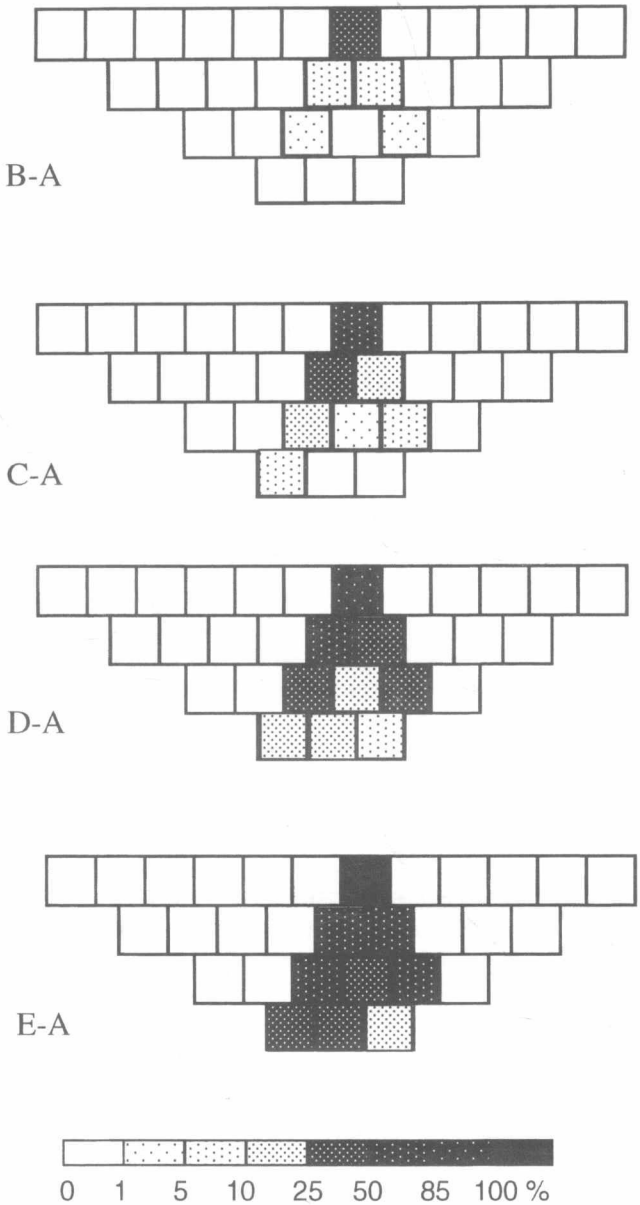

Fig. 8. Resistivity anomalies during the different stages along the profile.

hand. We did not expect variation of the top centimeters of the soil between the following cracking stages, though we did expect agreement between crack electrical signature and crack depth. The highest interpreted electrical resistivity was recorded in the top 1.5-cm depth, whereas the crack developed down to 4 cm. Similarly, Griffiths and Barker (1993) observed that detection and resolution both decreased with depth, setting limits on the degree of geological complexity. The actual interpreted data permitted to detect the presence of the crack, but did not allow predicting its depth. Crack depth variation was represented with a significant variation of the interpreted resistivity at the subsurface. These results led us to reconsider the inversion model: the Res2Dinv software cannot totally succeed in detecting abrupt structure geometry variations and strong electrical resistivity gradients because the numerical resolution of the mathematical algorithm is based on a regular mesh and a smoothness condition. However, this study suggests that even small structures, such as millimetric cracks, cause a significant change in resistivity distribution.

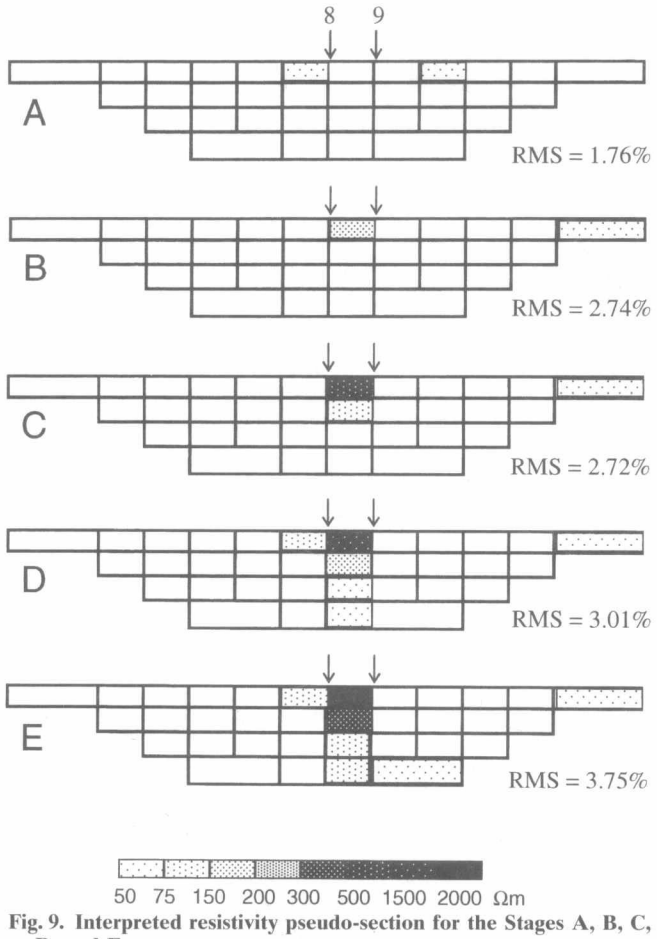

Fig. 9. Interpreted resistivity pseudo-section for the Stages A, B, C, D, and E.

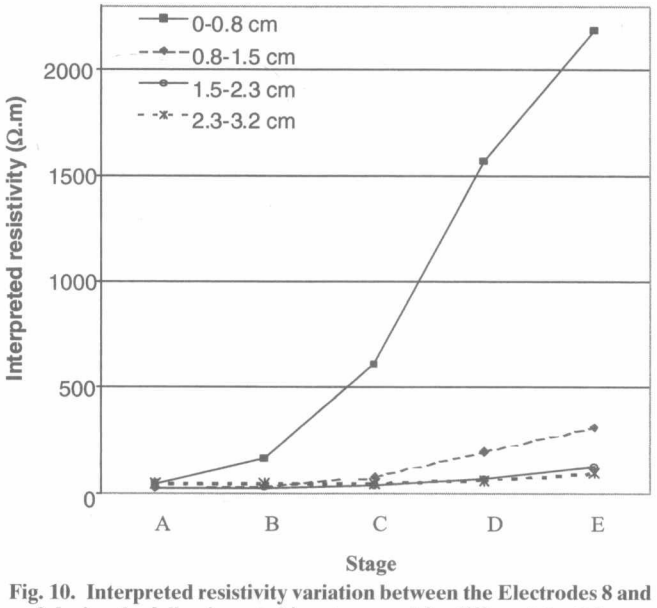

Fig. 10. Interpreted resistivity variation between the Electrodes 8 and 9 during the following cracking stages and for different depth investigation.

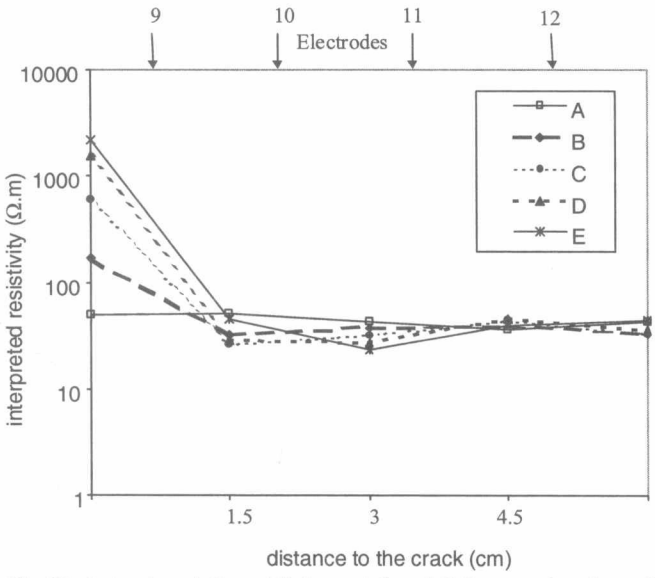

Fig. 11. Lateral variation of interpreted resistivity as a function of crack localization, for the first depth layer 0 to 0.8 cm.

CONCLUSION

The electrical resistivity image method is a relatively rapid method that can be used to investigate soil structure. The method produces a two-dimensional vertical section of interpreted electrical resistivity from the measurement of apparent resistivity. Our results demonstrate the effectiveness of electrical resistivity prospecting in characterizing soil cracks that form during shrinking and swelling phenomena at the centimetric scale. The $Cu/CuSO_4$ electrodes combined with a saturated ceramic cup permitted a correct electrical contact of the electrode with the soil surface. Regarding subsurface formation, the electrical images obtained from these electrodes enable detection of structures at the millimeter scale. This experiment is a first step in crack detection by using the electrical resistivity method.

Compared with other crack determination studies, the electrical resistivity method permits non-invasive measurements. These first results based on artificial cracks with two-dimensional imaging exploration are encouraging, but they confirm the need for future work on the inversion of the apparent resistivity data. Future work will consist in adapting this electrical monitoring to a soil block under desiccation condition to monitor a real crack network as it grows. Nevertheless, more detailed analysis of crack network requires appreciation of the entire volume of soil and not only of a two-dimensional section. Thus we will also develop a three-dimensional electrical resistivity set-up.

ACKNOWLEDGMENTS

The authors gratefully thank Keith Hodson for improving our English.

REFERENCES

Acworth, R.I. 1999. Investigation of dryland salinity using the electrical image method. Austr. J. Soil Res. 37:623–636.

Andrews, R.J., R. Barker, and L. Meng Heng. 1995. The application

of electrical tomography in the study of the unsatured zone in chalk at three sites in Cambridgeshire, United Kingdom. Hydrogeology J. 3:17–31.

Blackwell, P.S., M.A. Ward, R.N. Lefevre, and D.J. Cowan. 1985. Compaction of a swelling clay soil by agricultural traffic; effects upon conditions for growth of winter cereals and evidence for some recovery of structure. J. Soil Sci. 36:633–650.

Bourennane, H., D. King, R. Le Parco, M. Isambert, and A. Tabbagh. 1998. Three-dimensional analysis of soils and surface materials by electrical resistivity survey. Eur. J. Env. Eng. Geoph. 3:5–23.

Bullock, P., and C.P. Murphy. 1980. Toward the quantification of soil structure. J. Microsc. 120:317–328.

Chertkov, V.Y., and I. Ravina. 1998. Modeling the crack network of swelling clay soils. Soil Sci. Soc. Am. J. 62:1162–1171.

Dannowski, G., and U. Yaramanci. 1999. Estimation of water content and porosity using radar and geoelectrical measurements. Eur. J. Env. Eng. Geoph. 4:71–85.

Delapierre, A. 1998. Représentation en 3D d'une partie des vestiges d'une villa gallo-romaine à l'aide des méthodes életriques (Site gallo-romain d'Orbe-Boscéaz, Vaud, Suisse). (In French.) Mémoire de Master Institut de géophysique de Lausanne.

Edwards, L.S. 1977. A modified pseudosection for resistivity and IP. Geophysics 42:1020–1036.

Göbel, B., J. Michaelsen, E. Danchwardt, S.A. Hagrey, C. Meyer, G. Petzold, C. Stolte, and R. Thierbach. 1993. Geophysikalische Methoden zur Erfassung von Wasserverteilungen and Wassertransportvorgängen in Böden. (In German.) Mitteilgn. Deutsche. Bodenkundl. Gesellsch. 72:111–114.

Goyal, V.C., P.K. Gupta, P.K. Seth, and V.N. Singh. 1996. Estimation of temporal changes in soil moisture using resistivity method. Hydr. Proc. 10:1147–1154.

Griffiths, D.H., and R.D. Barker. 1993. Two-dimensional resistivity imaging and modelling in areas of complex geology. J. Appl. Geophysics 29:211–226.

Hagrey, S.A.A., and J. Michaelsen. 1999. Resistivity and percolation study of preferential flow in vadose zone at Bokhorst, Germany. Geophysics 64:746–753.

Hallaire, V. 1984. Evolution des reseaux de fissure lors du retrait d'un sol argileux. (In French.) (Cracks patterns evolution during shrinking in clayey soil) p. 323–327. *In* Fonctionnement hydrique et comportement des sols AFES, Dijon.

Hallaire, V. 1988. La fissuration d'un sol argileux au cours du dessèchement. II Modélisation morphologique (In French). Agronomie 8: 273–280.

Hesse, A., A. Jolivet, and A. Tabbagh. 1986. New prospects in shallow depth electrical surveying for archeological and pedological applications. Geophysics 51:585–594.

Horgan, G.W., and I.M. Young. 2000. An empirical stochastic model for the geometry of two-dimensional crack growth in soil (with discussion). Geoderma 96:263–276.

Lamotte, M., A. Bruand, M. Dabas, P. Donfack, G. Gabalda, A. Hesse, F.X. Humbel, and H. Robain. 1994. Distribution d'un horizon à forte cohésion au sein d'une couverture de sol aride du Nord-Cameroun: apport d'une prospection électrique (In French). C.R. Acad. Sci. 318:961–968.

Lima, L.A., and M.E. Grismer. 1992. Soil Crack Morphology and Soil Salinity. Soil Sci. 153:149–153.

Loke, M.H., and R.D. Barker. 1996. Rapid least-squares inversion of apparent resistivity pseudosections using a quasi-Newton method. Geophys. Prosp. 44:131–152.

Mackie-Dawson, L.A., C.E. Mullins, E.A. Fitzpatrick, and M.N. Court. 1989. Seasonal changes in the structure of clay soils in relation to soil management and crop type. I Effects of crop rotation at Cruden Bay. NE Scotland. J. Soil Sci. 40:269–281.

McGarry, D., B.J. Bridge, and B.J. Radford. 2000. Contrasting soil physical properties after zero and traditional tillage of an alluvial soil in the semi-arid subtropics. Soil Tillage Res. 53:105–115.

Michot, D., A. Dorigny, and Y. Benderitter. 2000. Mise en évidence par résistivité électrique des écoulements préférentiels et de l'assèchement par le maïs d'un calcisol de Beauce irrigué. (In French) C.R. Acad. Sci. 332:29–36.

Perrier, E., N. Bird, and M. Rieu. 1999. Generalizing the fractal model of soil structure: the pore-solid fractal approach. Geoderma 88: 137–164.

Richard, G., J.F. Sillon, and O. Marloie. 2001. Comparaison of inverse and direct evaporation methods for estomating soil hydraulic properties under different tillage practices. Soil Sci. Soc. Am. J. 65: 215–224.

Ringrose-Voase, A.J., and W.B. Sanidad. 1996. A method for measuring the development of surface cracks in soils: application to crack development after lowland rice. Geoderma 71:245–261.

Scollar, I., A. Tabbagh, A. Hesse, and I. Herzog. 1990. Archaeological prospecting and remote sensing. Cambridge Univ. Press, New York.

Scott, G.J.T., R. Webster, and S. Nortcliff. 1986. An analysis of crack pattern in clay soil: its density and orientation. J. Soil Sci. 37: 653–668.

Stadler, D., M. Stähli, P. Aeby, and H. Flühler. 2000. Dye tracing and image analysis for quantifying water infiltration into frozen soils. Soil Sci. Soc. Am. J. 64:505–516.

Stengel, P. 1988. Cracks formation during swelling: Effect on soil structure regeneration after compaction. p. 147–152. *In* Proc. 11th Conference of ISTRO, Edinburgh (Scotland). ISTRO, Haren, the Netherlands.

Tabbagh, A., M. Dabas, A. Hesse, and C. Panissod. 2000. Soil resistivity: A non-invasive tool to map soil structure horizonation. Geoderma 97:393–404.

Tuong, T.P., R.J. Cabangon, and M.C.S. Wopereis. 1996. Quantifying flow processes during land soaking of cracked rice soils. Soil Sci. Soc. Am. J. 60:872–879.

VandenBygaart, A.J., R. Protz, and A.D. Tomlin. 1999. Changes in pore structure in a no-till chronosequence silt loam soils, southern Ontario. Can. J. Soil Sci. 79:149–160.

Velde, B., E. Moreau, and F. Terrible. 1996. Pore networks in an italian Vertisol: Quantitative characterization by two dimensional image analysis. Geoderma 72:271–285.

Voorhees, W.B. 1983. Relative effectiveness of tillage and natural forces in alleviating wheel-induced soil compaction. Soil Sci. Soc. Am. J. 47:129–133.

Zhou, Q.Y., J. Shimada, and A. Sato. 2001. Three-dimensional spatial and temporal monitoring of soil water content using electrical resistivity tomography. Water Resour. Res. 37:273–285.

Estimating Temperature Effects on Water Flow in Variably Saturated Soils using Activation Energy

Fucang Zhang, Renduo Zhang,* and Shaozhong Kang

ABSTRACT

Temperature effects on soil water flow are attributable to various factors in the soil water system, such as fluid viscosity, soil water content, and other soil physical and chemical properties. To account for the factors as a whole and quantify the temperature effects, the first objective was to apply the concept of activation energy and to estimate apparent activation energies of steady-state saturated flow and horizontal as well as vertical infiltration. The second objective was to predict the water flow processes under different temperatures. Soil column experiments were conducted to measure discharge of steady-state saturated flow and processes of cumulative infiltration using four soils at four temperatures. The parameters of the flow equations were related to temperature and apparent activation energies. Based on the relationships, apparent activation energies of the water flow processes were estimated using the experimental data. The sensitivities of temperature effects on the steady-state saturated flow and infiltration parameters were linearly related to the activation energy and inversely proportional to the absolute temperature. In general, temperature effects on the water flow processes were larger in the fine-textured soils and/or with higher soil water saturation. Using the parameters estimated from measured water flow processes at two temperatures, we predicted the processes at other temperatures and compared the predicted results with the measured data. The predicted results were highly correlated with the measured data with coefficients of determination (r^2) larger than 0.990 and the relative errors of the predicted processes were within 12%.

THE EFFECT OF temperature on water flow processes in soils, such as infiltration and evaporation, has long been recognized. Some researchers have investigated variations in measured infiltration rates attributable to temperature changes. Bouwer et al. (1974) noted increased infiltration rates in a basin during summer vs. winter. Taking into account temperature dependence of soil hydraulic properties, Hopmans and Dane (1984) investigated the influence of soil temperature on soil water distributions during and after infiltration. Hopmans and Dane (1986) also simulated soil-water movement with different temperature regimes and boundary conditions. Jaynes et al. (1988) and Jaynes (1990) measured infiltration and soil temperature in the field and observed that the infiltration rate varied during a 24-h period, with a maximum in the late afternoon and a minimum in the early morning. Constantz and Murphy (1991) studied the temperature dependence of ponded infiltration and found that infiltration rate increased three to four-fold between 5 and 60°C for their soils. Based on measured cyclic seepage rates from unlined irrigation canals, Mitchell et al. (1990) related the 24-h cycle variation of seepage rates to the diurnal temperature variation of water.

Various factors in the soil water system, such as fluid viscosity, soil water content, and soil physical and chemical properties, interact with temperature changes in the system, therefore, influence the temperature effects on soil water flow processes. Some researchers (Constantz, 1982; Hopmans and Dane, 1986) related temperature dependence of the flow transport to the temperature change of liquid viscosity, which in turn affect soil water hydraulic conductivity. However, it was observed that using the temperature change of liquid viscosity only was inadequate to describe the influence of the temperature dependence of the matric potential. Other factors, such as the soil water surface tension and the diffuse double-layer thickness, may have a role in affecting the flow processes under different temperatures (Constantz, 1982).

To account for the various factors as a whole, the concept of apparent activation energies, which are necessary to overcome energy barriers in flow process, is a useful means to quantify the temperature effects on water flow processes in soils. The activation energy concept was introduced into the field of chemical kinetics by Arrhenius (1889) to explain the temperature dependence of sucrose hydrolysis rate in various acids. Glasstone et al. (1941) extended the concept to fluid flow processes to interpret the change of fluid viscosities and diffusion coefficients with temperature. Biggar and Taylor (1960) related an infiltration parameter to temperature with the Arrhenius equation, from which they estimated activation energies and described the observed temperature dependence of infiltration data. However, the temperature-dependent parameter used had no physical interpretation. Anderson et al. (1963) applied the concept of apparent activation energy to study temperature fluctuations at the wetting front and water movement in the liquid and vapor phases. They obtained apparent activation energies of 17.93, 25.18, and 25.39 kJ mol^{-1} for Palo Verde sandy loam, Arizona bentonite, and a muck soil, respectively. The results of apparent activation energies of Anderson et al. (1963) were significantly different from those by Biggar and Taylor (1960), which ranged from 4 to 12 kJ mol^{-1} for infiltration in various fractions of Millville silt loam were considered too low by Anderson et al. (1963). Therefore, it is necessary to further explore the spectrum of apparent activation energies for various soil water

F. Zhang and S. Kang, Key Lab. of Agricultural Soil and Water Engineering in Arid and Semiarid Areas, Northwest Science and Technology Univ. of Agriculture and Forestry, Yangling, Shaanxi, 712100, P.R. China; R. Zhang, Dep. of Renewable Resources, Univ. of Wyoming, Laramie, WY 82071-3354, USA. Also at Dep. of Water Resources, Wuhan Univ., Wuhan 430072, P.R. China; S. Kang, College of Water Resources and Civil Engineering, China Agriculture Univ., Beijing, 100083, P.R. China. Received 18 July 2002. *Corresponding author (renduo@uwyo.edu).

Published in Soil Sci. Soc. Am. J. 67:1327–1333 (2003).

677 S. Segoe Rd., Madison, WI 53711 USA

processes under different conditions. Furthermore, there is little attempt to utilize the activation energy concept to predict the temperature-dependent water flow processes in soils. Thus, the first objective of this study was to estimate apparent activation energies of water flow processes in saturated and unsaturated soils, from which we evaluated temperature effects on the water flow processes. The second objective was to predict the water flow processes under different temperatures, applying the concept of apparent activation energy. The predicted water flow processes were compared with experimental data.

MATERIALS AND METHODS

Water Flow Equations and Apparent Activation Energies

The steady-state flow in soils can be described by the Darcy equation:

$$Q = KA\nabla H \quad [1]$$

where Q is the discharge ($cm^3\ s^{-1}$), K is the hydraulic conductivity ($cm\ s^{-1}$), A is the cross-section area (cm^2), and ∇H is the hydraulic gradient ($cm\ cm^{-1}$). Eq. [1] can be expressed by

$$Q = \frac{K_0 \rho g}{\eta} A\nabla H \quad [2]$$

in which K_0 is the intrinsic hydraulic conductivity (cm^2), reflecting the effect of soil matrix on water flow, ρ is the fluid density ($g\ cm^{-3}$), g is the gravitational acceleration ($cm\ s^{-2}$), and η is the water viscosity ($g\ cm^{-1}\ s^{-1}$). The water viscosity changes with temperature, which may be quantified with the Arrhenius form of (Glasstone et al., 1941; Low, 1958)

$$\frac{1}{\eta} = b\exp\left(\frac{-E_v}{RT}\right) \quad [3]$$

Here b is a constant, E_v is the apparent activation energy ($J\ mol^{-1}$) for viscosity change of pure water, R is the gas constant ($8.31451\ J\ mol^{-1}\ K^{-1}$), and T is the absolute temperature in Kelvin. Assuming that the fluid density is independent of temperature, from Eq. [3] we have

$$Q = BA\nabla H\exp\left(-\frac{E_d}{RT}\right) \quad [4]$$

where B is a constant and E_d is the apparent activation energy ($J\ mol^{-1}$) of steady-state flow, which is a lumped parameter to account for factors having temperature effects on water flow, such as fluid viscosity, soil water content, and soil properties. Using Eq. [4] and plotting ln Q vs. $1/T$, we can evaluate E_d from the plot slope. In turn, Eq. [4] can be used to calculate steady state flow under different temperatures.

For horizontal infiltration, Philip (1957) gave the following approximation:

$$I(t) = St^{1/2} \quad [5]$$

where $I(t)$ is the cumulative infiltration (cm) within time t (s), S is the sorptivity ($cm\ s^{-1/2}$), relating to the soil matric potential. Vertical infiltration can be approximated by (Philip, 1957):

$$I(t) = St^{1/2} + A_0 t \quad [6]$$

where A_0 is the steady-state infiltration rate ($cm\ s^{-1}$), relating to the gravitational potential. The parameters in Eq. [5] and [6], S and A_0, change with temperature. According to Philip (1957), the soil sorptivity can be related to the soil water viscosity as follows

$$S^2 = \left(\frac{\sigma}{\eta}\cos\omega\right) S_i^2 \quad [7]$$

where σ is the surface tension ($N\ cm\ s^{-2}$), ω the contact angle in radian, S_i the intrinsic sorptivity ($cm\ s^{-1/2}$). Invoking Eq. [3], we may express the sorptivity with the Arrhenius equation in the form of (Anderson et al., 1963)

$$S^2 = F\exp\left(-\frac{E_s}{RT}\right) \quad [8]$$

where F is a constant, E_s is the apparent activation energy ($J\ mol^{-1}$) of infiltration attributable to the soil matric potential. The activation energy can be estimated from a plot of ln S^2 vs. $1/T$. The parameter A_0 is related to the gravitational potential and usually used to approximate the soil hydraulic conductivity. Therefore, similar to the derivation of Eq. [4], we can write the temperature change of A_0 in the following form:

$$A_0 = G\exp\left(-\frac{E_g}{RT}\right) \quad [9]$$

where G is a constant, E_g is the apparent activation energy ($J\ mol^{-1}$) of infiltration attributable to the gravitational potential.

Experiments

Four representative soils (designated with S1, S2, S3, and S4) collected in Shaanxi Province of China were used for the experiments. Some physical and chemical properties of the soils are listed in Table 1, such as particle-size distributions, soil classification, organic matter content, pH values, and cation-exchange capacity (CEC). The texture of the four soils ranged from loamy sand to sandy clay with clay content from 15 to 43%.

To prepare soil columns for the following experiments, we filled and packed the air-dried soil in a 1-cm interval into a soil column to keep a constant bulk density about $1.4\ g\ cm^{-3}$. More specifically, we calculated the weight of 1-cm depth of the soils based on the cross-sectional area of the soil column (4 cm in diameter) and the bulk density. The weighted soil was filled into the soil column and packed carefully to a depth of 1 cm. Then we brushed the soil surface to have a good contact with added soil and repeated the procedure. For vertical soil columns, ceramic plates with large pores were used at the bottom to hold the soil.

Steady-state flow experiments were conducted in vertical soil columns of 15 cm in length. To achieve complete saturation in the soil, the soil column was saturated from the bottom

Table 1. Physical and chemical properties of soils used for experiments.

Soil	Sand	Silt	Clay	Soil Classification	pH	Organic Matter	CEC
	%					$g\ kg^{-1}$	$cmol\ kg^{-1}$
S1	82	3	15	Loamy sand	8.2	2.9	4.48
S2	70	9	21	Sandy clay loam	7.8	9.1	10.17
S3	61	9	30	Sandy clay loam	8.0	11.4	17.28
S4	50	7	43	Sandy clay	6.8	5.8	21.35

using a positive pressure head. After the soil column was totally saturated, a 3.6-cm pressure head was kept at its top using a Mariotte bottle and the bottom was opened to the air. As the steady state was established with the constant pressure head (h) boundary conditions (h = 3.6 cm and 0 for the upper and lower boundaries, respectively), water collected from the bottom was used to calculate the discharge. The experiments were performed with the four soils and at four temperatures, 5, 20, 35, and 50°C. We set up one soil column for each of the soils and temperatures, totaling 16 soil columns. All experiments were conducted in a constant-temperature chamber with a temperature control precision ± 0.2°C. For each temperature, we repeated the experiment for five times using the same soil column.

Horizontal infiltration experiments were conducted in 20-cm long soil columns with a diameter of 5.8 cm. The inflow boundary was controlled at a −3.0-cm pressure head using a ceramic plate and a Mariotte bottle. Infiltrated water changing with time was measured from reading the graduated Mariotte bottle. The experiments were performed with the Soils S1 and S3 at four temperatures (5, 20, 35, 50°C). To verify gravity impact on soil water flow in the horizontal experiments, we plotted the cumulative infiltration vs. $t^{1/2}$ and fitted the data with a linear equation with a zero interception for each case of the different soils and temperatures. For all cases, the linear equations fitted the data extremely well with coefficients of determination $r^2 > 0.998$, which indicated that the gravity impact on soil water flow in the horizontal experiments was negligible.

Vertical infiltration experiments were conducted in 50-cm long soil columns with a diameter of 4.0 cm. The inflow boundary was controlled at a 2.0-cm pressure head using a graduated Mariotte bottle and infiltrated water changing with time was measured using the Mariotte bottle. The experiments were conducted with the Soils S1 and S3 at three temperatures (5, 20, 35°C). For the horizontal and vertical infiltration experiments, we set up one soil column for each of the soils and temperatures. Each experiment of the horizontal and vertical infiltration was repeated three times using the same column.

RESULTS AND DISCUSSION

Estimations of Apparent Activation Energies

Figure 1 presents the data of discharge of steady-state flow measured at different temperatures and in different soils. For all the measurements, the standard errors calculated based on the five measurements at each temperature were within 0.09 ($cm^3\ min^{-1}$) and the relative errors were <5%. With the consistent repeated measurements, we mainly concentrated on the average results of the data in the following discussions. Using Eq. [4] and the measured discharge data at different temperatures, we calculated apparent activation energies of the steady-state flow. We plotted ln Q vs. $1/T$ and obtained a linear relationship as follows:

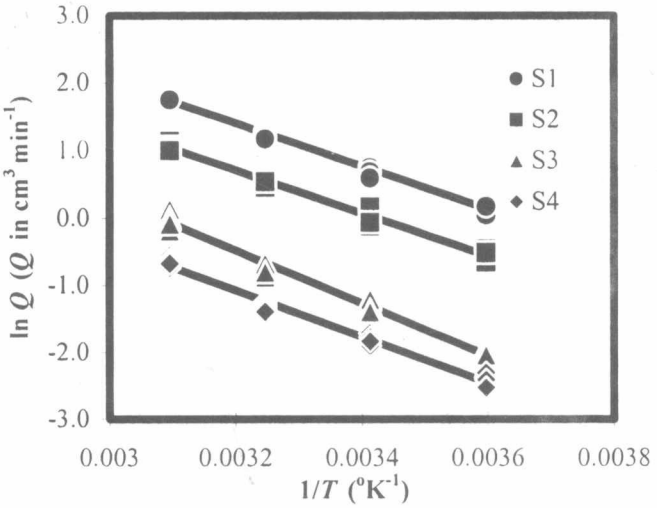

Fig. 1. The linear relationship between log of the discharge (ln Q) of steady-state saturated flow vs. $1/T$ (T: the absolute temperature).

$$\ln Q = a - \frac{E_d}{RT} \qquad [10]$$

where a is the intercept and E_d/R is the slope, from which we evaluated E_d. For example, for S1 we obtained E_d/R = 3182 °K, thus E_d = 26460 J mol^{-1} = 26.46 kJ mol^{-1} from the linear relationship with a coefficient of determination (r^2) of 0.9928 (Fig. 1). Results for other soils are summarized in Table 2.

Using a nonlinear optimization procedure (Marquardt, 1963) with the measured horizontal and vertical infiltration processes as well as Eq. [5] and [6], respectively, we obtained values of the infiltration parameters of S and A_0 at different temperatures. Note that sorptivity (S) is a function of soil water content. The sorptivity values calculated were the average results corresponding to the initial water content and supply water content. As an example, the temperature dependence of S calculated from the vertical infiltration processes is shown in Fig. 2, which includes the average S values based on the five measurements at each temperature and error bars. Using Eq. [8] and [9] and the estimated infiltration parameters, from the relationships of ln S^2 vs. $1/T$ and ln A_0 vs. $1/T$, we calculated the apparent activation energies of horizontal and vertical infiltration. The results are also listed in Table 2.

The apparent activation energies of the steady-state saturated flow are larger than those of infiltration (Table 2). The high apparent activation energies of the steady-state flow may result from the saturated soil water content, which affects the specific heat capacity of the soil water system. Van Duin (1963) showed that changing from a dry condition to the saturated condition, the heat capacity of a sand soil increased 2.86 times and the heat

Table 2. Apparent activation energies of different water flow processes.

Soil	Activation Energy	r^2
	kJ mol^{-1}	
	Steady State Saturated Flow	
S1	26.46	0.9928
S2	26.36	0.9976
S3	32.68	0.9943
S4	28.71	0.9963
	Horizontal Infiltration	
S1	13.13	0.9625
S3	13.57	0.9532
	Vertical Infiltration	
S1	17.02† (5.19)‡	0.9994† (0.9999)‡
S3	24.77 (10.34)	0.9714 (0.9880)

† Results calculated from Eq. [8].
‡ Results calculated from Eq. [9].